The Electrochemical Society
Advancing solid state & electrochemical science & technology

Editors' Choice—A Monolithic Photoelectrochemical Device Evolving Hydrogen in Pure Water

View the article online for updates and enhancements.

A Monolithic Photoelectrochemical Device Evolving Hydrogen in Pure Water

Tobias A. Kistler, [1,2,3] **Nemanja Danilovic,** [4,*] **and Peter Agbo** [1,2,z]

[1] *Chemical Sciences Division, Lawrence Berkeley National Laboratory, Berkeley, California, USA*
[2] *Joint Center for Artificial Photosynthesis, Lawrence Berkeley National Laboratory, Berkeley, California, USA*
[3] *Walter Schottky Institute and Physics Department, Technische Universität München, Garching, Germany*
[4] *Energy Storage and Distributed Resources Division, Lawrence Berkeley National Laboratory, Berkeley, California, USA*

We report the development of a fully-integrated, photoelectrochemical (PEC) device coupling water oxidation to hydrogen evolution using a III-V triple-junction photovoltaic (PV) embedded in a Nafion membrane. This architecture is genuinely monolithic, with wireless catalyst integration being achieved via compression of metal sputter-coated carbon electrodes against the front and back PV contacts. The resulting MEA-type, sandwich construct minimizes the path length for proton conduction through the membrane ionomer, while simultaneously preventing PV light attenuation by the catalyst layer, a common issue for monolithic PEC structures. Simulated, solar illumination of this construct, when operating in neutral-pH water, yields a peak solar-to-hydrogen efficiency of 12.6% during a four-day trial. While the wireless nature of monolithic PEC devices typically prevents the measurement of current flow and faradaic efficiencies, we circumvent this complication through the placement of an electrical shunt between the PV and the cathode catalyst layer, rerouting charge generated at the PV through a potentiostat prior to cathodic proton reduction. Using this configuration, we also show evidence of a corrosion current competing with anodic oxygen evolution under acidic conditions, highlighting the importance of quantifying product generation in monolithic devices.

Three decades of climate modeling conducted by the Intergovernmental Panel on Climate Change (IPCC) has highlighted the impact of carbon emissions on planetary warming, with damage mitigation efforts largely focused on transitioning the global energy sector away from fossil fuels.[1] Hydrogen, an energy carrier with a higher gravimetric energy density than gasoline,[2] represents a potential zero-carbon emission fuel, if it can be produced from renewable energy sources. In particular, photoelectrochemical (PEC) water splitting marks one of the most promising technologies for clean and renewable hydrogen production.[3–5] In a solar water splitting device, photons from the sun are collected using a photovoltaic (PV) cell, with the resulting photovoltage driving the endergonic oxidation of water to yield protons, which are then reduced to form hydrogen.[6] Design options for such devices range from integrated structures, where a photovoltaic element, placed in direct contact with the electrolyte of the electrochemical cell, forms a semiconductor-electrolyte junction (PEC architecture), to PV-electrolyzer units, where the light absorbing and electrochemical components are physically separated and connected through external wiring.

While promising, the implementation of photochemically-sourced hydrogen has been limited by economic constraints.[3] The U.S. Department of Energy (DOE) has set a target solar-to-hydrogen (STH) efficiency of 20% by 2020, with an ultimate target of 25% that corresponds to an equivalent cost of $2.10 per kg for hydrogen produced via photoelectrochemical methods (assuming PV costs of about $150–$200 per m^2).[7,8] Notable reports include devices displaying STH efficiencies of 12.4%[9,10] (later adjusted to 9.3%),[11] using the PEC architecture, and 18% in the PV-E configuration.[10,12] More recently, publications on PEC devices have demonstrated STH efficiencies of 14–19% using liquid electrolytes,[13–15] while PV-E devices have been demonstrated to reach higher efficiencies of over 30% with liquid electrolyte[16] and 15% using water vapor as reactant.[17]

Here, we provide characterizations of a monolithic device architecture featuring a III-V PV that has been embedded in a Nafion proton exchange membrane. Compression of carbon-supported platinum/iridium electrodes against the respective cathodic/anodic sides of the membrane-integrated, solar absorber yields a stable assembly of oxygen evolution reaction (OER) and hydrogen evolution reaction

(HER) catalysts with the Nafion-bound PV. Generally, fully-integrated devices require extreme pH electrolytes or supporting electrolytes to facilitate ion transport at macroscopic length scales without significant concentrations gradients and polarization losses.[18,19] In our photoelectrochemical system, ion transport distances are greatly reduced, thereby allowing operation using a neutral-pH feed without active circulation. The result is a compact, MEA-type device that is shown to couple water oxidation to hydrogen evolution at neutral pH upon solar irradiation, with STH efficiencies exceeding 12% under simulated AM1.5G illumination. Furthermore, the device stability is noteworthy, displaying an STH of 7% after four days of continuous, unbiased operation.

While traditionally, the design of monolithic PEC devices precludes any explicit measurement of electrical current during device operation,[20] we demonstrate a novel solution to this problem, through the placement of a shunt path between the PV and the cathode catalyst layer. Rerouting carriers through a potentiostat, placed in a series circuit between the PV and cathode catalyst elements, enabled direct monitoring of electrical current, with concomitant determination of real-time faradaic yields. These efforts revealed the existence of corrosive reactions that may compete with OER under certain conditions, suggesting that the assumptions of 100% faradaic yields that are often employed in the calculation of monolithic PEC STH efficiencies, must be made with caution.

Perhaps most critically, this study aims to address a broader challenge in the fabrication of photoelectrochemical devices: how may catalysts and catalyst supports developed for dark electrochemistry be effectively deployed in monolithic PEC device assemblies? The architecture outlined here provides a potential answer to this standing problem, with our PV-integrated membrane structure enabling the incorporation of carbon-supported, dark catalysts in a wireless, light-compatible scheme. This particular design also yields product-separated gas streams, obviating any requirement for downstream gas purification.

Experimental

Catalyst deposition.—Electrocatalysts were deposited by radio frequency (RF) sputtering in a 5-gun magnetron system onto carbon paper. The chamber was equipped with platinum (99.99%) and iridium (99.9%) targets, made in-house at Lawrence Berkeley National

Laboratory. Prior to sputter deposition, the untreated substrates were cleaned in a 30 mTorr atmosphere of Ar by plasma etching at 15 W for 5 min. Immediately after this treatment, a 100 nm layer of catalyst was deposited on an area of 1 cm^2, in an Ar plasma at 3 mTorr and 150 W. The thickness of deposited Ir (anode) and Pt (cathode) catalysts was controlled by monitoring the sputter deposition rate with a quartz crystal microbalance. Ir was deposited on both sides of the anodic carbon paper, while Pt covered the cathodic carbon paper only on the side facing the membrane, corresponding to a catalyst loading of 0.4 and 0.2 mg cm^{-2}, respectively. The catalysts, as well as the photovoltaic, have been chosen for demonstration purposes as they are well-studied. However, the device architecture introduced here should permit the integration of a range of materials,[21] depending on the specific application or goal.

Photovoltaic.—Commercially available, triple-junction solar cells (Type: Ultra Triple Junction, UTJ) from Spectrolab, Inc. (Sylmar, CA) with GaInP$_2$/InGaAs/Ge sub-cells on a Ge substrate, without the factory-made, anti-reflective coating on the top surface, were used to drive the photoelectrochemical (PEC) cell. The electrical data for the solar cell with the anti-reflective coating are available on the manufacturer's website.[22] The PV cells were diced into 1 × 1 cm^2 pieces, and a 2000 Å thick gold grid front contact and Au/Ag back contact was applied by Spectrolab to ensure proper current collection.

PV-integrated membrane (PIM) assembly.—First, a square hole is cut into the Nafion 115 membrane which is just slightly smaller than the III-V triple-junction PV described above, while a 1 mil thick tantalum foil is attached to the PV providing an extension of the PV front contact to the outside of the PEC device (Figure 1a). Next, the PV is centered on this hole and secured with a combination of Hysol (LOCTITE Hysol 9460) and EPO-TEK 302–3M epoxies (ratio 1:3, 'Hy-TEK'). This ratio yields ideal chemical resistance while providing desirable viscosity. After the glue has dried at room temperature

(a)　　　　　　　　　　　　　　　　　　　　(b)

(c)
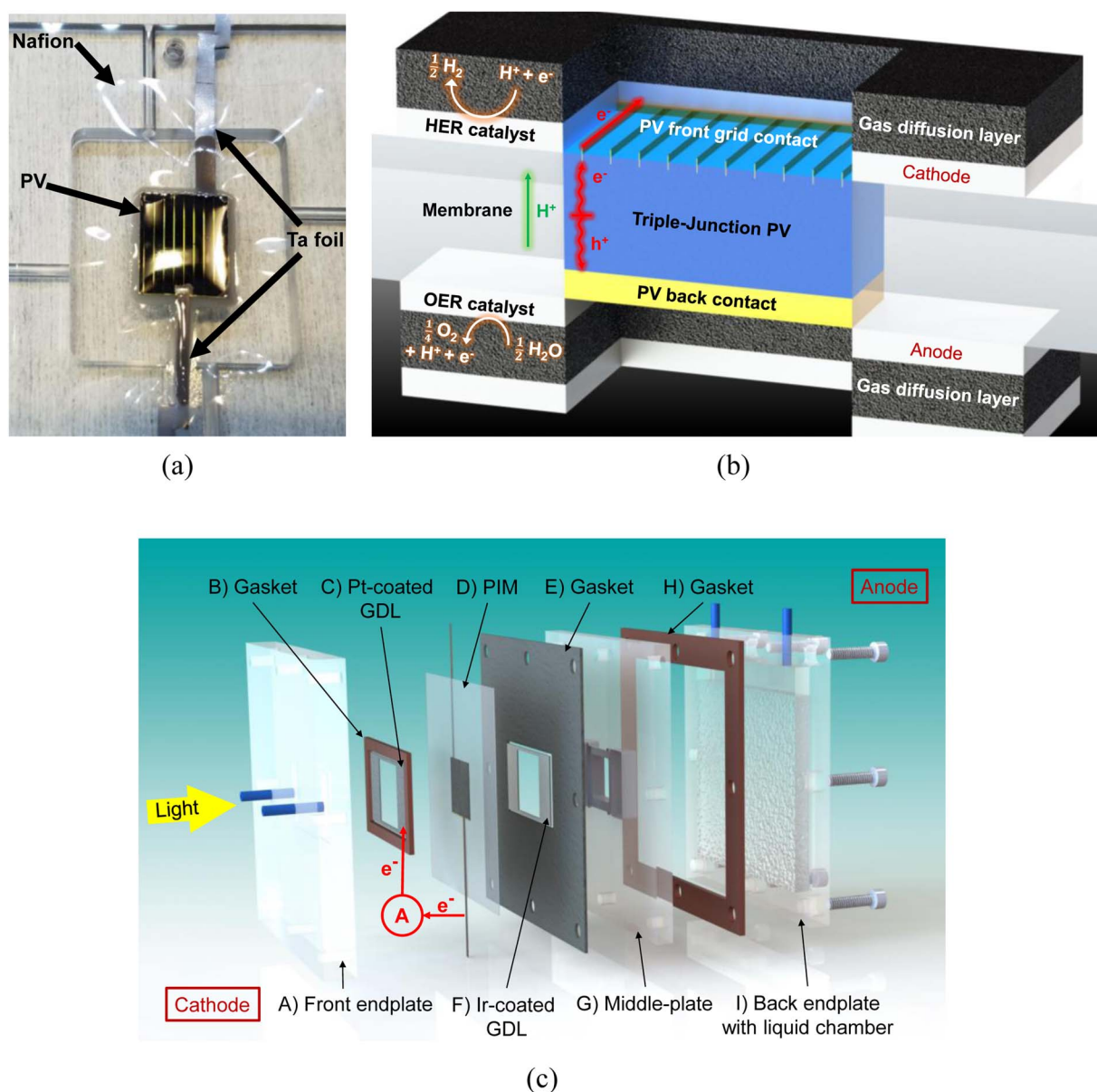
Figure 1. Essential components of the device architecture presented in this work (A) A triple-junction PV embedded into a Nafion membrane (PIM) serves as the core of the device. (B) A cross section of the photoelectrochemical cell's active components in the monolithic configuration (without wires). (C) Full assembly diagram of the monolithically-integrated PEC device, allowing for real-time current measurement and faradaic efficiency monitoring using a shunt path (marked red, detailed diagram in Figure S1).

for at least 12 hours, the tantalum foil attached to the PV front contact pad is secured with electrically conductive silver epoxy and dried at 60°C for 15 minutes. Then, the Hy-TEK epoxy mix is applied on the tantalum foil in order to electronically insulate it and allow for the establishment of an electrical shunt path required for real-time current monitoring (see Figure S1). The same silver epoxy procedure is repeated to establish a junction to the back of the PV and chemically sealed around the edges of the PV and over the silver epoxy with the Hy-TEK epoxy mix. Here, the part of the tantalum foil going to the back of the PV which is touching the membrane is left uncovered in order to allow for electrical contact to the anodic carbon paper. Finally, the front of the PV is covered with a thin layer of pure EPO-TEK epoxy which serves as both a corrosion-resistant[23,24] and anti-reflective coating (Figure S2).

After the PV-integrated membrane (PIM) has been manufactured, it is sandwiched between two pieces of Toray carbon paper sheets (2.17×1.22 cm^2 rectangle with a 1.21 cm^2 square hole, untreated TGP-H-60 carbon paper from Alfa Aesar, 0.20 mm thick) surrounding the PV (Figure 1b), serving dual roles as gas-diffusion layers (GDL) and catalyst supports. Charge carriers generated through light absorption by the solar cell migrate to the cathode and anode, driving the respective hydrogen and oxygen evolution reactions. Protons formed during water splitting at the iridium anode catalyst are transported through the Nafion ionomer to the cathode, yielding molecular hydrogen upon their reduction at the two-phase boundary formed by the membrane-catalyst junction. Immersion of the PV back contact in a liquid acting as a heatsink provides beneficial cooling for the PV surface under illumination conditions, increasing PV efficiency during operation.[25] Silicone gaskets serve as seals around the carbon catalyst supports, granting the requisite amount of compression to prevent fluid leakage from the cell and ensuring good contact between the catalysts and the membrane (Figure 1c). The device chassis is comprised of two transparent, polymethylmethacrylate (PMMA) endplates, plus a middle-plate serving as a support structure for the PIM and the carbon-supported electrocatalysts. The device here employs a low dead volume for the cathodic chamber ($\sim$40 mm^3), in order to reduce the latency period between hydrogen production and its subsequent detection. Meanwhile, the large-volume, anodic endplate ($\sim$5700 mm^3) serves as a liquid water reservoir.

Device performance measurements.—Before the unassisted stability measurements were started, CV curves were taken to examine the electrocatalytic (-2 V to 2.5 V, 0.2 V s^{-1}) and photovoltaic (0 to 2.6 V, 0.2 V s^{-1}) performance independently. Polarization sweeps also served to condition the catalysts, as iridium is partially oxidized during the course of electrochemical cycling.[26–28]

The photoelectrochemical cell was illuminated through the cathode using a solar simulator equipped with a Xe lamp and AM1.5G filter, providing a $12'' \times 12''$ illumination area. A reference cell with a monocrystalline silicon solar cell and an integrated thermocouple was used to determine the proper spatial position of the PEC device to ensure its exposure to a fixed light intensity of 1 sun (0.1 W cm^{-2}). This calibrated reference cell works most accurately when it is used to position solar cells with a similar bandgap ($\sim$1.1 eV). A subsequent comparison with higher bandgap reference cells indicated a 7% and $<$1% increase in illumination intensity for the GaInP$_2$ ($\sim$1.8 eV) and InGaAs ($\sim$1.3 eV) subcells, respectively. Measurements of the subcell quantum efficiencies suggest that the InGaAs subcell is current-limiting the PV and therefore, the illumination error is expected to be below 1%.

The product gases were analyzed every 7.5 min using a gas chromatograph (GC). A N$_2$ sweep gas flowed through a bubble humidifier at room temperature resulting in an output relative humidity (RH) of $\sim$70%. The humidified N$_2$ then flowed through the cathode compartment of the cell into a vapor water trap, with the gases accumulating in the trap's headspace being pushed into the GC. On the anode side, the electrolyte (Milli-Q water with a resistivity of $>$18.2 MΩ*cm) fills the liquid chamber and can access the anodic carbon paper through two holes (1.2×0.3 cm^2) machined into the middle-plate, while the

recessed ledge in the center of the middle-plate supports the PV from the anode side to prevent it from cracking during cell assembly and testing. Initially, the headspace of the anode's liquid reservoir was left open to the environment but was later sealed and purged with dry N$_2$ in order to measure the amount of O$_2$ production. The purge gases effectively increase the pressure in the electrode chambers because of the volumetric flow rate limitation in the GC. The gas flow rate was set to 2 sccm for the anode and 5 sccm for the cathode using mass flow controllers. It should be noted that the anode and cathode channels going to the GC could not be analyzed at the same time, and therefore, the two channels were alternately measured, with two subsequent injections being compared.

From the collected data, a solar-to-hydrogen efficiency (STH, Equation 1) can be calculated:

$$STH = \frac{\text{current density} \times 1.229 \text{ V} \times \text{faradaic efficiency}}{\text{illumination power density}} \quad [1]$$

We note that crossover hydrogen from the cathode to the anode and corrosion reactions effectively reduce the amount of produced H$_2$, which is reflected in the faradaic efficiency.

Results

Device characterization in neutral-pH water.—Performance results in pure water are shown in Figure 2, with the PEC device displaying good stability, despite the direct exposure of the semiconductor junction to the water in the anode. All STH efficiency values in the manuscript are based on the illuminated, photo-active area of the PV (1 cm^2). It is important to note that the semiconductor-liquid interface is an effective buried junction, with a factory-deposited Au back contact serving as the top-most layer of the PV's anode terminal.

Measurements of device J-V polarization curves (Figure 2a) reveal an onset voltage of ca. 1.5 V, slightly higher than the theoretical water oxidation voltage (1.229 V) due to resistive and kinetic losses. Overlays of the PV and electrolysis polarization curves yield an intersection providing the approximate operating point of the photoelectrochemical cell under steady-state conditions.[24,29] In this particular device, an overlap occurs around 1.8 V and 11 mA, at the beginning of operation, corresponding to a maximum STH efficiency of 13.5%, assuming a 100% faradaic efficiency for H$_2$ production.

Actual steady-state operation of the cell for four consecutive days results in an initial STH efficiency of 12.6%, which stabilizes between 7–9% for the remaining duration of a 96-hour trial (Figure 2b). The stoichiometry of the reaction products was constantly monitored, starting at the 25th hour of operation, when the anode compartment of the cell was sealed from the environment and a nitrogen carrier gas was pumped through its headspace. The expected H$_2$/O$_2$ ratio of 2 (2.08 $\pm$ 0.2) is verified through analysis of the concurrent GC measurements (Figure 2b), with the fluctuations in this value being attributed to cycles of oxygen bubble accumulation/desorption in the anode compartment. Furthermore, the calculation of product concentrations includes the device's outlet flow rates, which were fluctuating considerably during this experiment, possibly caused by water accumulation in the flow meters.

This particular device construction allows for simultaneous current measurement, which can be used to determine the device's faradaic efficiency in real time (Figure 2c). At the beginning of this test, when the anode was open to the environment, faradaic efficiencies of around 93% were measured. This value eventually increased to 98% after the anode was pressurized by the sweep gas flowing through its headspace. After the four-day operation, CV curves of PV and electrolysis were taken again (Figure 2a), showing a significant decrease in PV fill factor from 0.82 to 0.63 and open circuit voltage from 2.48 V to 2.34 V, corresponding to a PV efficiency drop from 22.5% to 16.3%. However, during this same period, the electrocatalytic performance is comparatively stable. The unassisted water splitting experiment represented in Figure 2b and Figure 2c was repeated twice more for a total of three independent trials, resulting in similar STH efficiencies for the device replicates (Figure 2d).
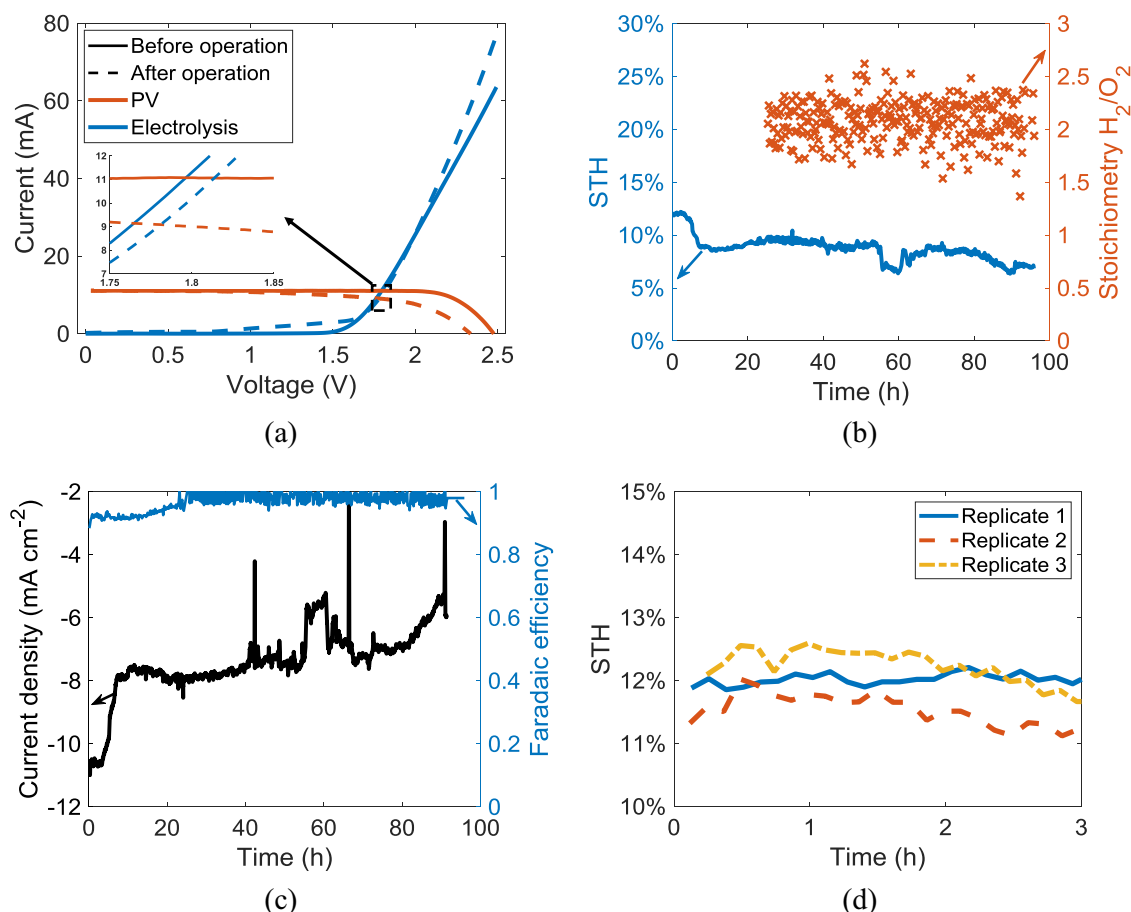
Figure 2. PEC device performance measurements display durable and efficient operation with a humidified (70% relative humidity) N_2 cathode feed and liquid water anode. (A) I-V curves of the PV before and after operation intersecting with the electrolysis CVs suggest minimal catalyst but appreciable PV degradation after the four-day operation. (B) Solar-to-hydrogen (STH) efficiency and product stoichiometry over the course of four days; though STH efficiency declined from 12% to 7%, H_2/O_2 product stoichiometry remains essentially constant at 2.08 ± 0.20 (oxygen product concentrations were first measured after 25 hours, when the anode was sealed). (C) Current density and faradaic efficiency monitoring using the electrical shunt circuit. The pressure increase resulting from sealing the anode leads to an enhancement in efficiency. Spikes in the current response mark the periodic addition of water to the anode. (D) STH efficiency of three device replicates show high degrees of reproducibility (number 1 represents the first three hours of the four-day experiment).

Investigations of device behavior under conditions of extreme pH conditions (0.1 M NaOH and 1 M H_2SO_4) were also conducted in efforts to reduce ionic transport losses and increase the electrolysis efficiency.[5,19,30] However, desirable durability was achievable at neither pH 0 nor pH 14, due to corrosion of the PV's back surface which was in direct contact with the anolyte (see Figure S3). If the buried, semiconductor-liquid junction was to be maintained, the suppression of PV corrosion demanded the use of neutral-pH water as the anolyte in the case of the III-V solar absorbers employed for this study.

Operation in true monolithic mode.—Following these trials, where direct current monitoring of the cell under solar illumination was used to characterize faradaic efficiency and corrosion processes, the device was tested without the presence of the electrical shunt circuit, to provide a demonstration of the cell operating as a traditional PEC monolith. Specifically, after the four-day trial, the cell was dismantled, the shunt path was removed, and the PIM device was reassembled using the same components, this time with the cathode catalyst in direct physical contact with the Au current collectors deposited on the front surface of the PV. In this fully-monolithic modality, where direct contact between the front PV contact and the Pt catalyst substrate was established, the device was illuminated for an additional 24 hours. During this test, STH efficiencies between 7–9% were determined (Figure 3), yielding values similar to the device's performance at the end of the preceding time trial, when current was monitored. The results verified the shunt circuit's role as a mere measurement appa-

ratus that is non-essential to device operation. Aside from serving as verification of genuine, monolithic operation without wires, this extended trial also indicated that the performance degradation is partially
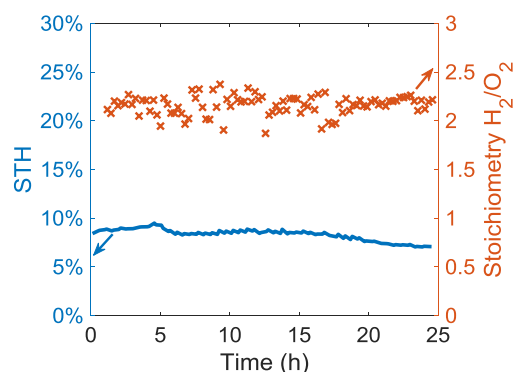
Figure 3. STH efficiency during the (true) monolithic testing period without current monitoring, confirming device operation without wires. Measurement conditions are the same as those reported in the 96-hour time trial where current was directly measured. The 2% increase in device STH efficiency observed, compared to the end of the four-day operation, suggests that the performance degradation originally seen may be partially reversible. The measured stoichiometry of product gases is stable at 2.16 ± 0.10.

reversible, with a ca. 2% recovery of device STH efficiency being observed. This reversible process is governed by the water-splitting overpotential which likely increases slightly during prolonged device operation, but recovers quickly afterwards. As a result of the dropping PV fill factor over the course of the 4-day experiment, an increasing water-splitting overpotential has a larger impact on device efficiency compared to a high fill factor PV.[23]

Discussion

Initial glances may suggest that PV-E architectures enjoy better prospects for market-scale deployment relative to their PEC counterparts, due to their (comparatively) straightforward scalability[31] and the relaxed constraints on component integration, particularly the freedom from having to consider the light attenuation and PV corrosion issues that make PEC device design so challenging. However, the integrated PEC device concept offers a unique array of possible advantages.[32,33] For example, a potential exists for using the electrolyte of the semiconductor-liquid junction as a heatsink that could enhance the device efficiency by cooling the photovoltaic under conditions of intense illumination.[25] Furthermore, the net-endothermic nature of OER-coupled, proton reduction may provide additional opportunities for thermal management of the PV temperature in fully-integrated systems – opportunities that are unavailable for the physically-separated PV and electrolyzer components found in PV-E systems.[5,34] Conversely, catalyst activity in integrated devices may benefit from the elevated temperatures caused by extended solar illumination, with such heat exchange processes being especially beneficial for catalyst performance under the increased temperatures induced by light concentration.[25] Device fabrication and assembly costs may also be reduced, as the external wiring and power-matching circuitry essential to PV-E systems would be absent from a monolithic PEC device.[35] Additionally, a PEC cell would not incur the possible external-circuit resistive losses associated with PV-E wiring, which may be non-negligible at the higher current densities (1–2 A cm^{-2}) where PV-E systems generally operate. Finally, the lower operating current densities of PEC devices result in an electrolysis efficiency that is generally higher than in PV-E systems,[36] opening the possibility of even low-cost, earth-abundant metals serving as realistic catalyst candidates. As a result, while fabrication is particularly challenging, it is conceivable that full realization of the monolithic PEC device concept may yield the economically preferred route for solar hydrogen production.

Stable catalyst integration.—At the low ionic strengths of neutral pH, it becomes especially important to minimize ohmic losses in order to achieve sustained hydrogen evolution.[18] Compressing two identically-sized, carbon paper catalyst supports against the membrane lowers the ionic path length for proton conduction. The net effect is a reduction in resistive losses, with a corresponding enhancement of electrocatalyst performance.[20,37] In addition, this device is shown to reduce the risk of bubble cavitation-induced, catalyst delamination, as seen in the provided time-lapse video of device operation (Supplemental Material). Notably, large oxygen bubbles are found to slowly accumulate at the top of the two holes in the middle-plate of the anodic chamber, rather than rapidly fume from the catalyst layer, a process known to result in material delamination. Scanning electron microscope images corroborate this observation of minimal perturbation to the catalyst layer following device operation (Figure S4). Hence, carbon gas-diffusion layer degradation does not seem to be an issue at the anode. However, for long-term use in industrial applications, it may be necessary to replace these carbon supports with more robust, Ti-based, gas diffusion layers.[5,25,38]

Stability comparison with the literature.—While higher, initial STH efficiencies have been reported previously,[13–15] most reported devices lack the stability displayed by the PIM device described here. In Figure 4, the reported current densities over time are compared with the PIM monolith. It should be noted that this device incorporates a photo-active area about one order of magnitude larger than
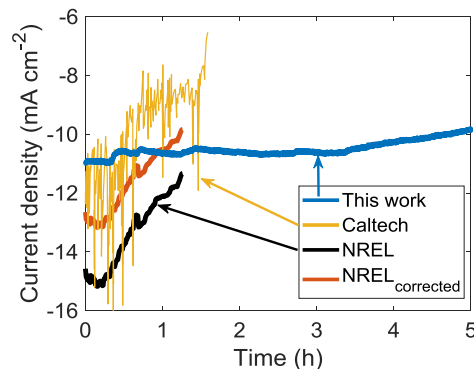
Figure 4. Stability comparison with high efficiency devices previously reported by NREL[13] and Caltech.[14] Results from NREL[13] were rescaled (red trace) based on their reported, maximum efficiency as previously suggested by Cheng et al.[14] Original NREL data in shown in black.

either of the reports we compare against.[13,14] For the device from May et al.,[15] unbiased, two-electrode configuration data was only available for 2 minutes and is therefore not plotted here. The current reported by Young et al.[13] (NREL) is rescaled based on their reported, maximum STH efficiency of 16.2%, as previously suggested by Cheng et al.[14] (Caltech). After one hour, the device from this work exhibits a performance that compares favorably to current reports in the literature,[13–15] while showing stable performance for several more hours. Traditionally, catalysts in monolithic PEC devices are placed directly on top of the solar absorber, leading to limitations in terms of durability and light attenuation. The improved stability of this device is largely attributed to our use of a neutral-pH anolyte and a mode of catalyst integration inspired by dark electrochemistry. The lower, initial STH efficiency can readily be increased using a PV providing a current exceeding 11 mA cm^{-2} at the operating point.

Faradaic efficiency – a key factor in assessing device performance.—The initial STH efficiency of 12% is slightly lower than the estimated efficiency of 13.5% gathered from the intersection of electrolysis and PV curve in Figure 2a. This discrepancy, caused by sub-unity faradaic efficiencies, is especially pronounced at the beginning of the measurement. However, this is found to be an artifact of delayed hydrogen detection in the GC, caused by the degree of physical separation between the point of H$_2$ evolution and detection, and the low flow rate of produced gas. While during the second injection into the GC, after 7.5 minutes, product concentrations have reached nearly 95% of their final values, it takes roughly one hour for full concentration equilibrium in the GC, as evidenced during the calibration of the GC. By the first, equilibrated hydrogen detection time point, electrical current has already dropped slightly compared to the initial current. Furthermore, hydrogen product crossover causes a reduction of the faradaic efficiency throughout the whole experiment. Hydrogen crossover depends on the temperature, the membrane thickness[23] and also the pressure difference[39,40] between the two electrode compartments. During the first 25 hours of the four-day experiment, the anode was at environmental pressure, while the cathode was pressurized due to the connection to the GC, limiting the volumetric flow rate. The pressure difference between cathode and anode increased the hydrogen crossover rate, resulting in a faradaic efficiency of 93% that eventually peaked at 98%, after pressurization of the anode. This is supported by a constant hydrogen crossover rate of 2% measured in the anode stream, which onsets after 25 hours of device testing.

Furthermore, corrosion reactions of the PV can compete with oxygen evolution at the anode, creating the illusion of a high STH efficiency, where hydrogen is produced at faradaic efficiencies near 100% without being coupled to water oxidation (Figure S3). The possibility of corrosive shunts kinetically competing with OER (or conceivably HER) highlights the importance of explicitly measuring faradaic yields in PEC device performance tests.[41,42] In addition to corrosion-induced

efficiency drops, it was observed that device operation at low current densities on the order of 1 mA cm^{-2} could lead to significant dehydration of the Nafion membrane, also resulting in reduced faradaic efficiencies (Figure S5).

Conclusions

While PEC device performances have yet to achieve the requisite durability and scalability needed for real-world deployments, advances in the field of photoelectrochemistry continue to show promise. In service of this goal, we have detailed the characterization of a fully-integrated device architecture that allows for both efficient and durable hydrogen production driven by a renewable power source. An initial STH efficiency of 12% was achieved, which slowly decreased to 9% after 50 hours and 7% after 4 days using a PV with an efficiency of 22.5%. More efficient, commercially-available PVs providing higher current densities, can readily increase the STH efficiency of this device, while the catalysts may be replaced by cheaper alternatives, facts pointing to the inherent modularity of the PIM device structure.

We aimed to address practical issues associated with PEC devices. In particular, this study demonstrates a strategy for incorporating catalysts and catalyst supports developed for dark electrochemistry in an integrated, wireless, light-compatible scheme. For the purpose of this work, the catalyst area on the carbon paper equaled the PV area (1 cm^2). However, during scale-up, the catalyst area could be reduced relatively to the PV area, using more efficient, commercially-available catalyst layers to increase the illuminated PV area. Furthermore, the device architecture presented is not limited to hydrogen evolution, as virtually any electrochemical process may be incorporated, provided that suitable membrane, catalyst and solar absorbing components are chosen. Finally, this device configuration allowed illumination through the cathode of the device. Such a configuration was beneficial, as irradiation through the gas-phase cathode chamber significantly reduced drops in device performance caused by path-dependent light attenuation.

Our incorporation of an optional electrical shunt structure allowed for real-time measurement of electrical current and the continuous extraction of faradaic yields, factors which proved essential in eliminating potential misinterpretation of STH efficiencies, while advancing our device optimization efforts. Faradaic efficiencies for hydrogen and oxygen are often assumed to be 100% in PEC device literature, leading to possible overestimations of STH efficiency under non-ideal conditions. The results of our study prompt recommendations that future PEC device reports quantify both product gas streams, as such data can provide useful insights into the existence of possible corrosive currents impacting device behavior. An improved comprehension of such processes may grant a window into how they may be suppressed, paving the way to PEC devices with significantly improved operation lifetimes.

ORCID

Tobias A. Kistler   https://orcid.org/0000-0001-6458-8024
Peter Agbo   https://orcid.org/0000-0003-3066-4791

References

1. M. Allen, M. Babiker, Y. Chen, H. De Coninck, S. Connors, R. van Diemen, O. P. Dube, K. L. Ebi, K. Ebi, F. Engelbrecht, and M. Ferrat, *Global warming of 1.5°C*, IPCC, Geneva, Switzerland (2018).
2. C. Jiang, S. J. A. Moniz, A. Wang, T. Zhang, and J. Tang, *Chem. Soc. Rev.*, **46**, 4645 (2017).
3. E. L. Miller, *Energy Environ. Sci.*, **8**, 2809 (2015).
4. D. Jing, L. Guo, L. Zhao, X. Zhang, H. Liu, M. Li, S. Shen, G. Liu, X. Hu, and X. Zhang, *Int. J. Hydrogen Energy*, **35**, 7087 (2010).
5. M. Carmo, D. L. Fritz, J. Mergel, and D. Stolten, *Int. J. Hydrogen Energy*, **38**, 4901 (2013).
6. M. Grätzel, *Nature*, **414**, 338 (2001).
7. J. W. Vickers, H. N. Dinh, K. Randolph, A. Z. Weber, A. H. McDaniel, R. Boardman, T. Ogitsu, H. Colon-Mercado, D. Peterson, and E. L. Miller, *ECS Trans.*, **85**, 3 (2018).
8. B. A. Pinaud, J. D. Benck, L. C. Seitz, A. J. Forman, Z. Chen, T. G. Deutsch, B. D. James, K. N. Baum, G. N. Baum, S. Ardo, H. Wang, E. Miller, and T. F. Jaramillo, *Energy Environ. Sci.*, **6**, 1983 (2013).
9. O. Khaselev and J. A. Turner, *Science*, **280**, 425 (1998).
10. J. W. Ager, M. R. Shaner, K. A. Walczak, I. D. Sharp, and S. Ardo, *Energy Environ. Sci.*, **8**, 2811 (2015).
11. H. Döscher, J. L. Young, J. F. Geisz, J. A. Turner, and T. G. Deutsch, *Energy Environ. Sci.*, **9**, 74 (2016).
12. S. Licht, B. Wang, S. Mukerji, T. Soga, M. Umeno, and H. Tributsch, *J. Phys. Chem. B*, **104**, 8920 (2000).
13. J. L. Young, M. A. Steiner, H. Döscher, R. M. France, J. A. Turner, and T. G. Deutsch, *Nat. Energy*, **2**, 453 (2017).
14. W.-H. Cheng, M. H. Richter, M. M. May, J. Ohlmann, D. Lackner, F. Dimroth, T. Hannappel, H. A. Atwater, and H.-J. Lewerenz, *ACS Energy Lett.*, **3**, 1795 (2018).
15. M. M. May, H.-J. Lewerenz, D. Lackner, F. Dimroth, and T. Hannappel, *Nat. Commun.*, **6**, 8286 (2015).
16. J. Jia, L. C. Seitz, J. D. Benck, Y. Huo, Y. Chen, J. W. D. Ng, T. Bilir, J. S. Harris, and T. F. Jaramillo, *Nat. Commun.*, **7**, 13237 (2016).
17. G. Heremans, C. Trompoukis, N. Daems, T. Bosserez, I. F. J. Vankelecom, J. A. Martens, and J. Rongé, *Sustainable Energy Fuels*, **1**, 2061 (2017).
18. M. A. Modestino, K. A. Walczak, A. Berger, C. M. Evans, S. Haussener, C. Koval, J. S. Newman, J. W. Ager, and R. A. Segalman, *Energy Environ. Sci.*, **7**, 297 (2013).
19. K. Sun, R. Liu, Y. Chen, E. Verlage, N. S. Lewis, and C. Xiang, *Adv. Energy Mater.*, **6**, 1600379 (2016).
20. W. J. C. Vijselaar, P. Perez-Rodriguez, P. J. Westerik, R. M. Tiggelaar, A. H. M. Smets, H. Gardeniers, and J. Huskens, *Adv. Energy Mater.*, **9**, 1803548 (2019).
21. R. Gao and D. Yan, *Adv. Energy Mater.*, **180**, 1900954 (2019).
22. https://www.spectrolab.com/photovoltaics/UTJ_CIC_Data_Sheet.pdf.
23. T. A. Kistler, D. Larson, K. Walczak, P. Agbo, I. D. Sharp, A. Z. Weber, and N. Danilovic, *J. Electrochem. Soc.*, **166**, H3020 (2019).
24. K. A. Walczak, G. Segev, D. M. Larson, J. W. Beeman, F. A. Houle, and I. D. Sharp, *Adv. Energy Mater.*, **7**, 1602791 (2017).
25. S. Tembhurne, F. Nandjou, and S. Haussener, *Nat. Energy*, **4**, 399 (2019).
26. S. Siracusano, V. Baglio, S. A. Grigoriev, L. Merlo, V. N. Fateev, and A. S. Aricò, *J. Power Sources*, **366**, 105 (2017).
27. A. Ganassin, V. Colic, J. Tymoczko, A. S. Bandarenka, and W. Schuhmann, *Phys. Chem. Chem. Phys.*, **17**, 8349 (2015).
28. D. N. Buckley, L. D. Burke, and J. K. Mulcahy, *J. Chem. Soc., Faraday Trans.* **1**, **72**, 1896 (1976).
29. C. Xiang, K. Walczak, J. Haber, R. Jones, J. W. Beeman, D. Guevarra, C. Karp, R. Liu, M. Shaner, K. Sun, W. West, and L. Zhou, in *Integrated Solar Fuel Generators, I. D. Sharp, H. A. Atwater and H.-J. Lewerenz, Editors, p. 387*, Royal Society of Chemistry, Cambridge, UK (2018).
30. J. Luo, D. A. Vermaas, D. Bi, A. Hagfeldt, W. A. Smith, and M. Grätzel, *Adv. Energy Mater.*, **6**, 1600100 (2016).
31. W. J. Chang, K.-H. Lee, H. Ha, K. Jin, G. Kim, S.-T. Hwang, H.-m. Lee, S.-W. Ahn, W. Yoon, H. Seo, J. S. Hong, Y. K. Go, J.-I. Ha, and K. T. Nam, *ACS Omega*, **2**, 1009 (2017).
32. E. Verlage, S. Hu, R. Liu, R. J. R. Jones, K. Sun, C. Xiang, N. S. Lewis, and H. A. Atwater, *Energy Environ. Sci.*, **8**, 3166 (2015).
33. R. van de Krol and B. A. Parkinson, *MRS Energy & Sustainability*, **4**, 146 (2017).
34. G. Peharz, F. Dimroth, and U. Wittstadt, *Int. J. Hydrogen Energy*, **32**, 3248 (2007).
35. A. J. Bard and M. A. Fox, *Acc. Chem. Res.*, **28**, 141 (1995).
36. S. Haussener, S. Hu, C. Xiang, A. Z. Weber, and N. S. Lewis, *Energy Environ. Sci.*, **6**, 3605 (2013).
37. J. Newman, *J. Electrochem. Soc.*, **160**, F309 (2013).
38. M. Bernt, A. Siebel, and H. A. Gasteiger, *J. Electrochem. Soc.*, **165**, F305 (2018).
39. K. D. Baik, B. K. Hong, and M. S. Kim, *Renewable Energy*, **57**, 234 (2013).
40. Y. S. Kim and K.-S. Lee, *Polym. Rev.*, **55**, 330 (2015).
41. F. Nandjou and S. Haussener, *ChemSusChem*, **12**, 1984 (2019).
42. Z. Chen, T. F. Jaramillo, T. G. Deutsch, A. Kleiman-Shwarstein, A. J. Forman, N. Gaillard, R. Garland, K. Takanabe, C. Heske, M. Sunkara, E. W. McFarland, K. Domen, E. L. Miller, J. A. Turner, and H. N. Dinh, *J. Mater. Res.*, **25**, 3 (2010).